Geophysical Research Letters

RESEARCH LETTER
10.1029/2019GL086941

Distinct Orogenic Processes in the South- and North-Central Tien Shan From Receiver Functions

Bingfeng Zhang[1], **Xuewei Bao**[1], **and Yixian Xu**[1]

[1]Key Laboratory of Geoscience Big Data and Deep Resource of Zhejiang Province, School of Earth Sciences, Zhejiang University, Hangzhou, China

Key Points:
- Detailed crustal structure beneath the Central Tien Shan is imaged, suggesting varying deformation processes perpendicular to its strike
- The shortening and thickening of the Tien Shan crust are responsible for the high elevations in the South-Central Tien Shan
- The underthrusting of the Kazakh Shield beneath the North-Central Tien Shan accommodates the convergence there

Supporting Information:
- Supporting Information S1
- Table S1

Correspondence to:
X. Bao,
xwbao@zju.edu.cn

Citation:
Zhang, B., Bao, X., & Xu, Y. (2020). Distinct orogenic processes in the south- and north-central tien shan from receiver functions. *Geophysical Research Letters*, *47*, e2019GL086941. https://doi.org/10.1029/2019GL086941

Received 31 DEC 2019
Accepted 1 MAR 2020

Abstract Uplifting mechanisms for the Tien Shan, an active intracontinental orogenic belt, have been under debate for decades, a key issue being how the convergence has been accommodated at depth. Here we investigate the Moho structure across the Central Tien Shan by common-conversion-point imaging and H-k-c stacking of receiver functions from a dense array. The observed Moho exhibits distinct characteristics among subblocks. A southward-dipping diffuse Moho is imaged in the South-Central Tien Shan (SCTS), in contrast with the relatively flat and sharp Moho beneath the Tarim Basin. This feature along with the large Moho offset beneath the South-Boundary Fault suggests that the shortening and thickening of the Tien Shan crust rather than the underthrusting of the Tarim Basin are responsible for the uplift of the SCTS. In the North-Central Tien Shan, however, the imaged Moho doublet provides direct evidence for the underthrusting of the Kazakh Shield accommodating the convergence there.

Plain Language Summary The formation of the Tien Shan mountains, situated ~1,500 km north of the plate boundary between India and Eurasia, has puzzled scientists for decades. Tectonic activities at depth could deform and thus leave footprints on subsurface interfaces such as the crust-mantle boundary (Moho). In this study, we reveal distinct Moho structure in the southern and northern parts of the Central Tien Shan through analyses of seismic records, suggesting different mountain building processes in the two regions. The strong Tarim Basin to the south squeezes the weak South-Central Tien Shan mass just as a wooden block squeezes plasticine. The Kazakh lower crust in the north, on the other hand, underthrusts beneath the North-Central Tien Shan. The combined effects of the two processes lead to the rapid growth of the present-day Tien Shan.

1. Introduction

The Tien Shan, one of the largest and most active intracontinental orogenic belts on Earth, has undergone tectonic uplift since 20–25 Ma (Sobel & Dumitru, 1997; Yin et al., 1998) in response to the collision between India and Eurasia (Molnar & Tapponnier, 1975). Deformation is distributed pervasively across the mountains, accommodated by active thrust faults on the edge of and within the belt (Thompson et al., 2002; Zubovich et al., 2010). Geographically, the Central Tien Shan is bounded by two stable tectonic units, the Tarim Basin to the south and the Kazakh Shield to the north, and can be divided into three segments: the North-Central Tien Shan (NCTS), the Middle-Central Tien Shan (MCTS), and the South-Central Tien Shan (SCTS) based on Paleozoic fault zones (Figure 1).

The high relief in the Tien Shan mountains is the product of compressional tectonics; however, it remains an enigma regarding the geodynamic processes at depth, which are responsible for this surface reconstruction. Several hypotheses have been proposed based on geophysical findings. The underthrusting of the Tarim and Kazakh lithosphere beneath the Tien Shan has been suggested by high-velocity anomalies in the upper mantle (Koulakov, 2011; Lei, 2011; Lei & Zhao, 2007), thickened mantle transition zone (Chen et al., 1997; Tian et al., 2010; Yu et al., 2017), and wave speed reversal in the lower crust (Gilligan et al., 2014; Sychev et al., 2018). However, the northward underthrusting of the Tarim Basin has been questioned by a deep seismic-reflection profile in the Central Tien Shan (Gao et al., 2013) and a receiver function (RF) investigation in the Eastern Tien Shan (Li, Zhang, et al., 2016). Interestingly, recent studies also show no clear evidence for the southward underthrusting of the Tarim Basin beneath the Tibetan Plateau (Bao et al., 2015; Kao et al., 2001; Yang & Liu, 2002).

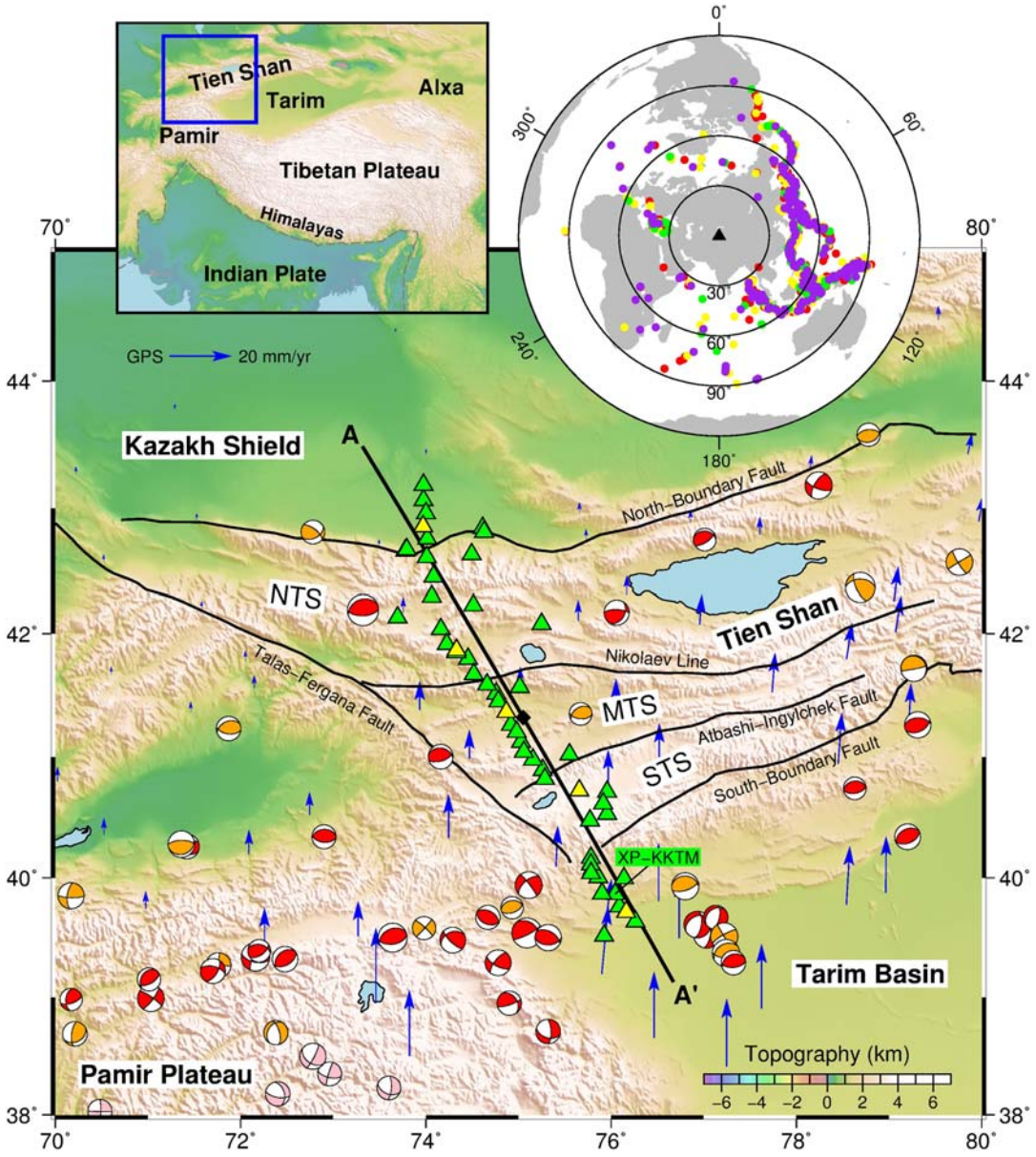

Figure 1. Topography map of the Central Tien Shan. Black thin lines show major fault zones and sutures separating main tectonic segments: the North-Central Tien Shan (NCTS), the Middle-Central Tien Shan (MCTS), and the South-Central Tien Shan (SCTS). Stations are marked as triangles with the ones shown in Figures 2, S1, and S2 labeled or colored in yellow. Line A-A′ shows the projected profile in Figure 3. The top right inset illustrates the back-azimuthal distribution of teleseismic events (purple: MANAS, yellow: KRNET, green: GHENGIS, and red: KNET) whereas the top left panel shows the study area in a larger scale. Blue arrows denote GPS velocities relative to Eurasia (Zubovich et al., 2010). Beach balls show focal mechanisms for large earthquakes ($M_b > 5.5$) since 1976 (Ekström et al., 2012) where event depths are indicated by different colors (red: 0–20 km, orange: 20–50 km, and pink: 50–150 km).

Structural information on subsurface interfaces, such as the Moho, is a good indicator of deformation and dynamics at depth. Previous studies suggest that the depth of the Moho varies significantly across the Tien Shan, ranging from 45 to 75 km (Bump & Sheehan, 1998; Gilligan et al., 2014; Kumar et al., 2005; Li, Shi, & Gao, 2016; Steffen et al., 2011; Vinnik et al., 2004). However, due to limited resolution and sensitivity of the utilized methods and/or data, the detailed morphology of the Moho beneath the Tien Shan remains unclear. In order to evaluate the abovementioned hypotheses and deepen our understanding of the orogenic processes in the Tien Shan, RFs derived from an orogen-perpendicular array of closely spaced seismograph stations are used to image the Moho with unprecedented details, offering fresh insights into the deformation patterns of compressional intracontinental orogens.

2. Data and Methods

Data used in this study are mainly from a dense passive-source seismic array of the Middle AsiaN Active Source project (Makarov et al., 2010). This deployment consisted of 40 broadband seismograph stations along a NNW-SSE trending profile across the Central Tien Shan with an interstation spacing of ~10 km (Figure 1). To better image the Moho interface, the Middle AsiaN Active Source data are supplemented with seismograms from KNET, KRNET, and GHENGIS networks. We select teleseismic events with good signal-to-noise ratios, magnitudes $\geq$ 5.5, and epicentral distances between 30° and 95°, and remove free-surface effects from three-component seismograms using the wave-vector method (Reading et al., 2003; Svenningsen & Jacobsen, 2004). Then, we calculate radial RFs using the time-domain iterative deconvolution approach (Ligorría & Ammon, 1999), which applies a Gaussian low-pass filter to suppress high-frequency noise (>1 Hz). All the RFs with good fit (>70%) are visually inspected in FuncLab (Porritt & Miller, 2018). A total of 9,247 RFs (corresponding to 1,223 teleseismic events) are finally obtained, which provide an overall good coverage in both distance and azimuth of the analyzed data (Figure 1). Supporting Information Figure S1 plots the waveforms of RFs of several representative stations.

To obtain detailed morphology of the Moho discontinuity, an image section for Profile A-A′ is constructed by the common-conversion-point (CCP) stacking technique (Zhu et al., 2006). Every amplitude on the RFs is assumed to be generated by a P-to-S conversion on a seismic discontinuity and projected into the depth domain along the theoretical ray path determined using the CRUST 1.0 model (Laske et al., 2013). The existence and properties of seismic discontinuities are detected based on the conversion amplitudes that depend on the magnitudes and signs of velocity contrasts.

We also estimate crustal thickness (H) and Vp/Vs ratio (k) at each station using a modified H-k stacking scheme with harmonic corrections (H-k-c) (Li et al., 2019; Zhu & Kanamori, 2000). The algorithm resolves and removes the degree-1 and degree-2 back-azimuthal harmonic variations of Moho Ps and two crustal multiples and then performs the traditional H-k scheme on the harmonic-corrected RFs to calculate the optimal solution of H and k. Standard deviations are estimated using the bootstrapping resampling technique (Efron & Tibshirani, 1986). In such a highly deformed orogenic belt, the traditional H-k method often suffers from severe trade-off and multiple peaks on the energy maps. The H-k-c scheme, on the other hand, reduces the ambiguity on the energy maps by removing the back-azimuthal effects of anisotropic media and dipping interface on the three phases, thus generating more robust measurements of H and k (Figure S2). An example of H-k-c analysis at station XP-KKTM is shown in Figure 2.

3. Results

The most prominent feature in the CCP image (Figure 3c) is the lateral variation of Moho conversions between 30- and 70-km depth, which is also evident in Figure 3b between 5 and 9 s. The Moho morphology correlates well with major tectonic segments across the profile. In the southern margin of the Kazakh Shield, the Moho conversions appear at approximately 45-km depth and plunge into the southern margin of the NCTS at a low angle. The Tien Shan Moho can be divided into three segments based on its geometry and sharpness, corresponding to the division of the mountains. The NCTS is characterized by Moho doublet with the Kazakh lower crust underthrusting beneath the Tien Shan. The apparent "gap" of the underthrusted Kazakh Moho conversions beneath the center of the NCTS is probably caused by small-scale heterogeneities of the crust (Figure S3), and the Kazakh lower crust likely extends beneath the whole NCTS. The Moho conversions in the MCTS are strong and relatively flat at approximately 46-km depth while those in the SCTS gradually become diffuse and dip southward to 65- to 70-km depth. Further south, an offset of Moho appears beneath the South-Boundary Fault (SBF) with the Tarim Moho lying at approximately 50-km depth. Intracrustal positive conversions in the Kazakh Shield (~19 km) and the Tarim Basin (~28 km) indicate two-layered crust in both regions. No explicit conversions associated with intracrustal discontinuities are observed in the mountainous Tien Shan.

We obtain 49 reliable measurements (Table S1) of crustal thickness and Vp/Vs ratio from H-k-c analysis. Four stations are discarded due to large back-azimuthal gaps or unreasonable results compared to adjacent stations. The crustal thicknesses show significant variations along the profile, ranging from 44 to 70 km with an average of 54 km (Figure 3c). The deepest Moho is observed at station XP-KORU in the SCTS while the shallowest is located at station XP-CHIC in the southern margin of the Kazakh Shield. The resulting Moho

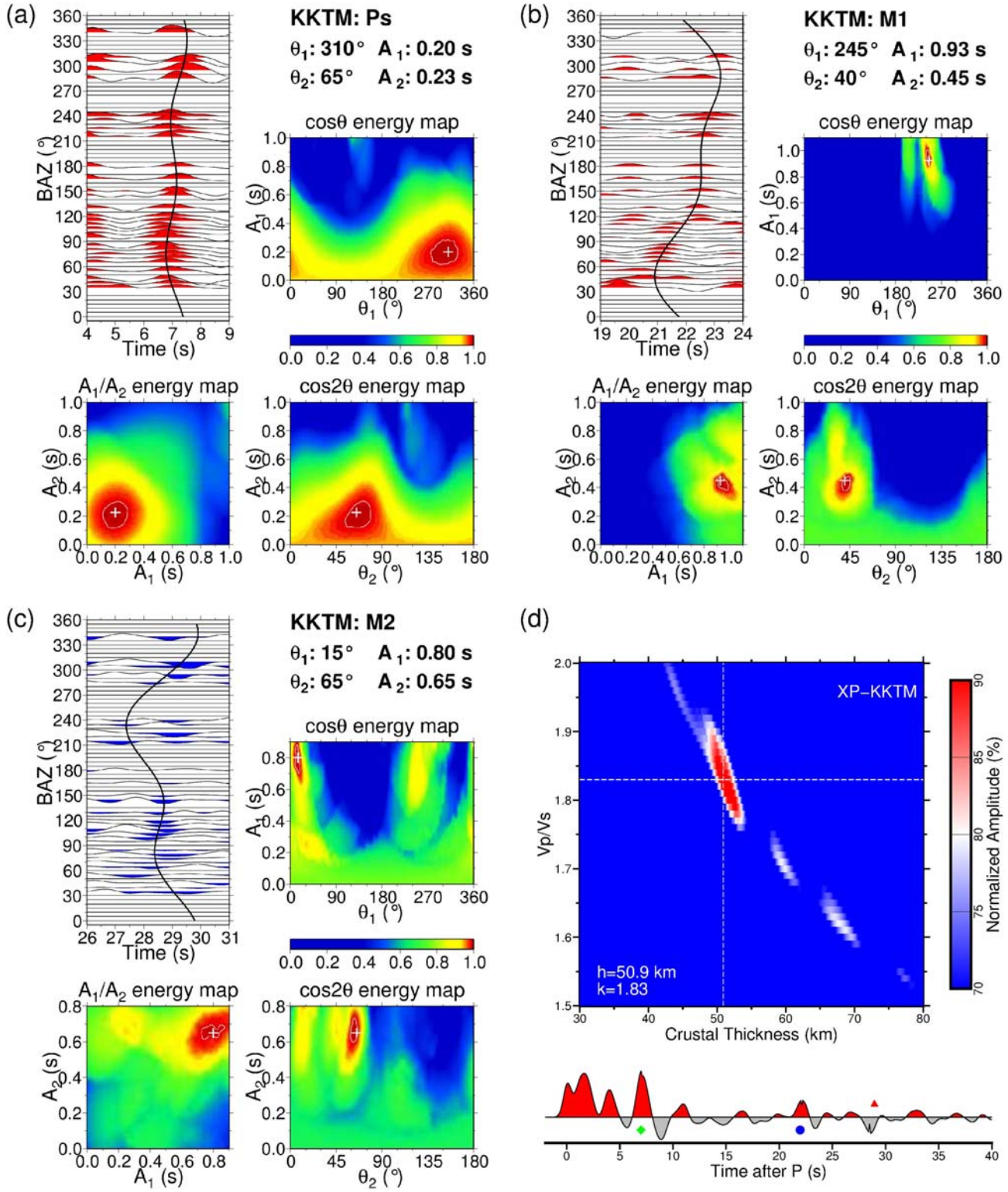

Figure 2. An example of H-k-c analysis at station XP-KKTM. (a–c) Best-fit harmonic fitting curves with cosθ and cos2θ functions, search results of harmonic parameters, and energy maps showing the optimal harmonic parameters for the three phases (Ps, M1(PpPs), M2 (PpSs + PsPs)). Uncertainties are shown by 99% contour lines on the energy maps. The good alignment of the best-fit harmonic curves and the three phases ensures the removal of harmonic effects, arising particularly from crustal anisotropy and dipping Moho. (d) Top: energy map showing the optimal crustal thickness and Vp/Vs ratio. Bottom: stack of harmonic-corrected receiver functions. The green, blue, and red symbols indicate the Ps, M1, and M2 phases, respectively.

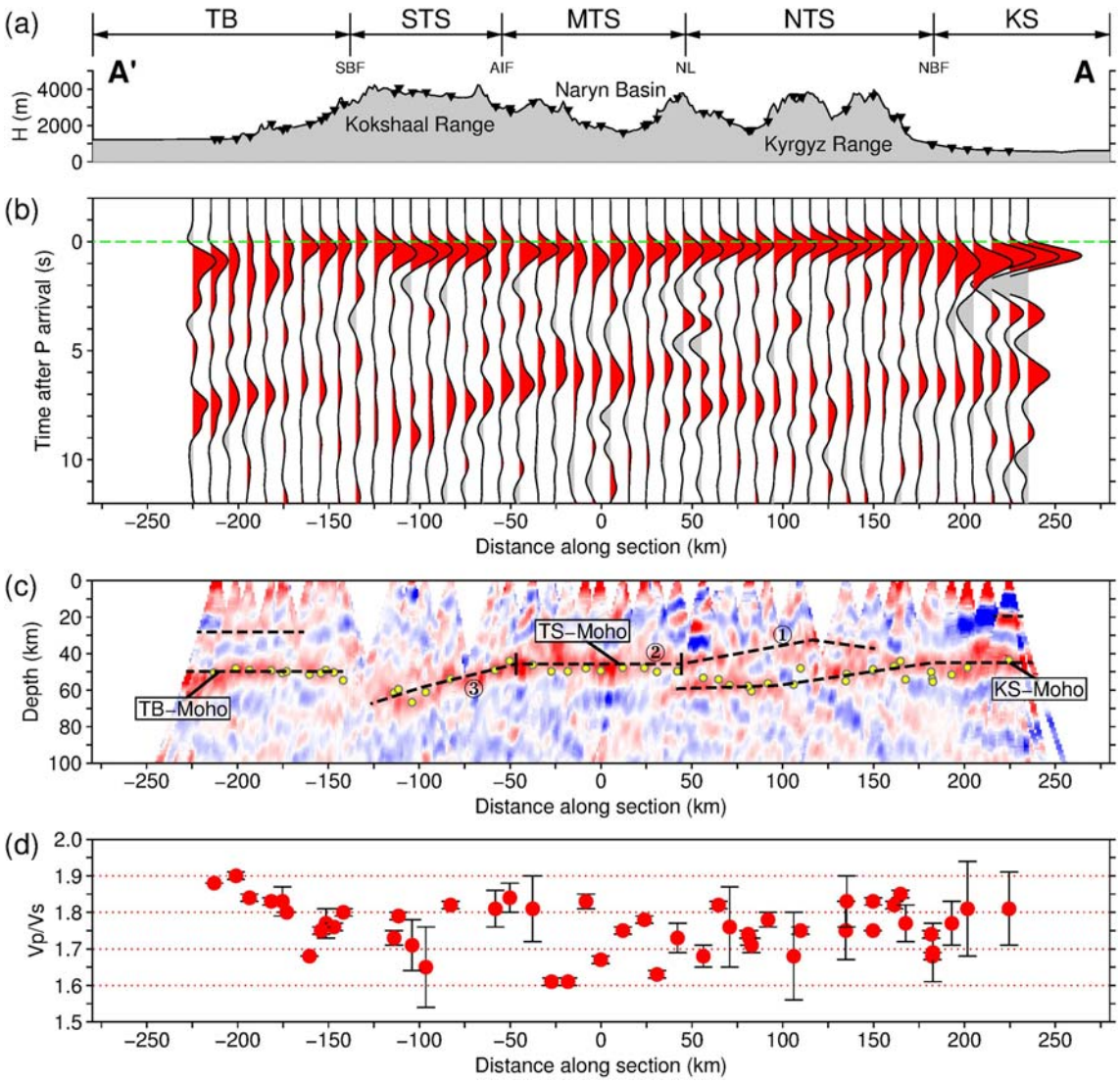

Figure 3. (a) Surface relief along profile A-A′. Major tectonic segments separated by faults or sutures are labeled (TB: the Tarim Basin, SCTS: the South-Central Tien Shan, MCTS: the Middle-Central Tien Shan, NCTS: the North-Central Tien Shan, KS: the Kazakh Shield, SBF: South-Boundary Fault, AIF: Atbashi-Ingylchek Fault, NL: Nikolaev Line, and NBF: North-Boundary Fault). (b) Stacked receiver function image obtained by binning and stacking the moveout-corrected receiver functions according to their piercing locations at Moho depths, which are determined by the CRUST 1.0 model (Laske et al., 2013). Moho Ps conversions with lateral variations are explicitly observed between 5 and 9 s. (c) Image showing the CCP results. Red and blue colors show positive and negative amplitudes, respectively. Moho depths obtained by H-k-c analysis are marked by yellow circles, consistent with the Moho conversions from CCP analysis. Black dashed lines denote the preferred Moho geometry, which show significant variations in different tectonic segments. (d) Vp/Vs ratio measurements from H-k-c analysis. Uncertainties are marked by black bars.

depths generally agree with the Moho conversions in the CCP image (Figure 3c), which enhances the credibility of the imaged Moho structure. The H-k-c-based Moho correlates with the deeper conversions of the Moho doublet in the NCTS, suggesting larger velocity gradient at the Kazakh Moho depth. The Vp/Vs ratio measurements vary from 1.61 to 1.90 with a standard deviation of 0.03 (Figure 3d). The Tarim Basin and the Kazakh Shield are characterized by high Vp/Vs ratios (~1.80) likely due to the thick sediments, whereas the average Vp/Vs ratio of the Tien Shan is ~1.75, suggesting limited occurrence of partial melt in the crust.

4. Discussion

Although previous studies inferred similar variations of the Moho depth beneath the Central Tien Shan (Gilligan et al., 2014; Li, Shi, & Gao, 2016; Makarov et al., 2010; Vinnik et al., 2004) as we describe above,

our CCP image illuminates the geometry of the Moho with more details, such as the Moho offset beneath the SBF and the Moho doublet beneath the NCTS, which provides fresh insights into the orogenic processes of the Tien Shan.

The northward subduction of the Tarim lithosphere has been supposed to account for the thickened crust and uplift in the SCTS (Gilligan et al., 2014; Makarov et al., 2010; Vinnik et al., 2006). However, our CCP image (Figure 3c) shows distinct Moho structure in the SCTS and the Tarim Basin. The SCTS Moho conversions are diffuse and dip southward while the Tarim counterparts are relatively flat and sharp. Based on this feature as well as the large Moho offset beneath the SBF, we conjecture that the underthrusting of the Tarim Basin is unlikely the dominant collisional process between the Tien Shan and the Tarim Basin. This interpretation is in agreement with a deep seismic-reflection profile (Gao et al., 2013), which suggests that thrust faults and décollements beneath the northernmost Tarim Basin are confined above the cratonic crystalline basement at approximately 24-km depth, equivalent to the upper-lower crustal interface shown in Figure 3c.

We suggest instead that the shortening and thickening of the SCTS crust are responsible for the high relief there. The Tarim Moho is well preserved during the orogenic processes while the SCTS crust, on the other hand, experiences intense deformation (Figure 3c). Such distinct responses to compressional tectonics may be controlled by the large lithospheric strength contrast between the SCTS and the Tarim Basin (Bagdassarov et al., 2011; Flesch et al., 2001). The northward subhorizontal indentation and obstruction of the strong Tarim lithosphere have resulted in the thickening of the SCTS crust and its uplift. Some Paleozoic faults originating during the Paleozoic Tarim-Tien Shan collisional event (Simonov et al., 2008) may also be reactivated during this orogenic process, thus forming the active Keping fold-thrust belt in the northern margin of the Tarim Basin.

The Moho doublet in the NCTS (Figure 3c) provides direct evidence for the low-angle southward underthrusting of the Kazakh lower crust contributing to the uplift there. This inference is also supported by several body wave tomography investigations (Koulakov, 2011; Lei & Zhao, 2007), which indicated that the Kazakh lithosphere dips southward to approximately 200-km depth beneath the Tien Shan. The lower crustal conversion at depths between 30 and 40 km beneath the NCTS corresponds well to the high-velocity layer revealed by joint inversion of surface wave dispersion and RFs (Gilligan et al., 2014; Li, Shi, & Gao, 2016). The high-velocity lower crustal layer beneath the NCTS may be due to mafic/ultramafic composition (Li, Shi, & Gao, 2016), pressure increase, and/or partial eclogitization of the underthrusted Kazakh lower crust. It is noteworthy that a recent RF image also revealed that the southward underthrusting of the Junggar Basin beneath the Eastern Tien Shan (Li, Zhang, et al., 2016), indicating that the southward underthrusting of the adjacent stable terranes beneath the Northern Tien Shan has played an important role in the uplift of the northern part of the mountains.

Relatively flat Moho and low surface relief in the MCTS suggest that this region has experienced minor deformation in the Cenozoic in comparison with the NCTS and SCTS, thus forming the sedimentary basin. Sparse seismicity in the interior of the Naryn Basin (Engdahl et al., 1998) also confirms the stability of the MCTS crust. Magnetotelluric and RF studies (Bielinski et al., 2003; Oreshin et al., 2002; Vinnik et al., 2006) revealed the high strength of the MCTS mantle lithosphere based on its high resistivity and high velocity, which was interpreted as an ancient platform remnant. This strong lithospheric lid could transfer stress from SCTS to NCTS and block potential upwelling mantle flow, thus protecting the overlying crust from considerable deformation.

Quantitative estimates of the Cenozoic shortening in the Central Tien Shan have mainly focused on the SCTS-Tarim foreland (Heermance et al., 2008; Scharer et al., 2004) while the cumulative shortening estimates (Avouac et al., 1993; Li, Zhang, et al., 2016; Makarov, 1995) across the mountains exhibit considerable discrepancy ranging from 50 to 203 km with large uncertainties. The morphology of the Central Tien Shan Moho shown in Figure 3c can be used to estimate the amount of crustal shortening. In detail, ~110 km of the shortening is accommodated by the Moho overlap in the NCTS while ~20 km is absorbed in the SCTS by crustal thickening if we assume the original crustal thickness equals to that of the weakly deformed MCTS. Geodetic studies (Abdrakhmatov et al., 1996; Zubovich et al., 2010) suggested that the Tarim Basin converges with the Kazakh Shield at ~20 mm year^{-1}, which is significantly higher than the average shortening rate of ~6 mm year^{-1} estimated from the total Cenozoic shortening amount of ~130 km, indicating a recent acceleration of deformation. This inference is in agreement with the pulsed deformation since

the Late Miocene in the NCTS (Bullen et al., 2003) and pre-Miocene shortening rate of ~3 mm year^{-1} across the Tien Shan (England & Molnar, 2015).

5. Conclusions

In this study, high-resolution Moho structure across the Central Tien Shan is obtained using RF techniques and can be divided into three segments. The diffuse and southward-dipping Moho conversions are imaged in the SCTS with a large offset from the flat Tarim counterpart beneath the SBF. The relatively flat Moho at approximately 46-km depth and the Moho doublet are observed in the MCTS and NCTS, respectively. A total crustal shortening of ~130 km is estimated by the imaged Moho morphology. The new information about the Moho structure provides constraints on the crustal deformation pattern of the Central Tien Shan. We suggest that the shortening and thickening of the SCTS crust and the underthrusting of the Kazakh Shield are the dominant orogenic processes in the southern and northern parts of the Central Tien Shan, respectively.

Acknowledgments
We are grateful to the Editor Lucy Flesch and the two anonymous reviewers for their constructive comments, which greatly improved the manuscript. We thank Lupei Zhu and Jiangtao Li for sharing their codes and Xiaodong Song for comments on the early draft. Waveform data are archived and provided by IRIS Data Management Center (http://ds.iris.edu/ds/nodes/dmc/). Most figures are prepared using Generic Mapping Tools (GMT) software (Wessel et al., 20132013). This study is supported by the National Natural Science Foundation of China (41774045 and 41830212) and the Fundamental Research Funds for the Central Universities.

References

Abdrakhmatov, K. Y., Aldazhanov, S. A., Hager, B. H., Hamburger, M. W., Herring, T. A., Kalabaev, K. B., et al. (1996). Relatively recent construction of the Tien Shan inferred from GPS measurements of present-day crustal deformation rates. *Nature*, *384*(6608), 450–453. https://doi.org/10.1038/384450a0

Avouac, J. P., Tapponnier, P., Bai, M., You, H., & Wang, G. (1993). Active thrusting and folding along the northern Tien Shan and Late Cenozoic rotation of the Tarim relative to Dzungaria and Kazakhstan. *Journal of Geophysical Research*, *98*(B4), 6755–6804. https://doi.org/10.1029/92jb01963

Bagdassarov, N., Batalev, V., & Egorova, V. (2011). State of lithosphere beneath Tien Shan from petrology and electrical conductivity of xenoliths. *Journal of Geophysical Research*, *116*, B01202. https://doi.org/10.1029/2009jb007125

Bao, X., Song, X., & Li, J. (2015). High-resolution lithospheric structure beneath mainland China from ambient noise and earthquake surface-wave tomography. *Earth and Planetary Science Letters*, *417*, 132–141. https://doi.org/10.1016/j.epsl.2015.02.024

Bielinski, R. A., Park, S. K., Rybin, A., Batalev, V., Jun, S., & Sears, C. (2003). Lithospheric heterogeneity in the Kyrgyz Tien Shan imaged by magnetotelluric studies. *Geophysical Research Letters*, *30*(15), 1806. https://doi.org/10.1029/2003gl017455

Bullen, M. E., Burbank, D. W., & Garver, J. I. (2003). Building the Northern Tien Shan: Integrated thermal, structural, and topographic constraints. *The Journal of Geology*, *111*(2), 149–165. https://doi.org/10.1086/345840

Bump, H. A., & Sheehan, A. F. (1998). Crustal thickness variations across the Northern Tien Shan from teleseismic receiver functions. *Geophysical Research Letters*, *25*(7), 1055–1058. https://doi.org/10.1029/98gl00516

Chen, Y. H., Roecker, S. W., & Kosarev, G. L. (1997). Elevation of the 410 km discontinuity beneath the Central Tien Shan: Evidence for a detached lithospheric root. *Geophysical Research Letters*, *24*(12), 1531–1534. https://doi.org/10.1029/97gl01434

Efron, B., & Tibshirani, R. (1986). Bootstrap methods for standard errors, confidence intervals, and other measures of statistical accuracy. *Statistical Science*, *1*(1), 54–77. https://doi.org/10.1214/ss/1177013815

Ekström, G., Nettles, M., & Dziewoński, A. M. (2012). The global CMT project 2004–2010: Centroid-moment tensors for 13,017 earthquakes. *Physics of the Earth and Planetary Interiors*, *200-201*, 1–9. https://doi.org/10.1016/j.pepi.2012.04.002

Engdahl, E. R., van der Hilst, R., & Buland, R. (1998). Global teleseismic earthquake relocation with improved travel times and procedures for depth determination. *Bulletin of the Seismological Society of America*, *88*(3), 722–743.

England, P., & Molnar, P. (2015). Rheology of the lithosphere beneath the central and western Tien Shan. *Journal of Geophysical Research: Solid Earth*, *120*, 3803–3823. https://doi.org/10.1002/2014jb011733

Flesch, L. M., Haines, A. J., & Holt, W. E. (2001). Dynamics of the India-Eurasia collision zone. *Journal of Geophysical Research*, *106*(B8), 16,435–16,460. https://doi.org/10.1029/2001jb000208

Gao, R., Hou, H., Cai, X., Knapp, J. H., He, R., Liu, J., et al. (2013). Fine crustal structure beneath the junction of the Southwest Tian Shan and Tarim Basin, NW China. *Lithosphere*, *5*(4), 382–392. https://doi.org/10.1130/l248.1

Gilligan, A., Roecker, S. W., Priestley, K. F., & Nunn, C. (2014). Shear velocity model for the Kyrgyz Tien Shan from joint inversion of receiver function and surface wave data. *Geophysical Journal International*, *199*(1), 480–498. https://doi.org/10.1093/gji/ggu225

Heermance, R. V., Chen, J., Burbank, D. W., & Miao, J. (2008). Temporal constraints and pulsed Late Cenozoic deformation during the structural disruption of the active Kashi foreland, northwest China. *Tectonics*, *27*, TC6012. https://doi.org/10.1029/2007tc002226

Kao, H., Gao, R., Rau, R.-J., Shi, D., Chen, R.-Y., Guan, Y., & Wu, F. T. (2001). Seismic image of the Tarim Basin and its collision with Tibet. *Geology*, *29*(7), 575–578. https://doi.org/10.1130/0091-7613(2001)029<0575:siottb>2.0.co;2

Koulakov, I. (2011). High-frequency P and S velocity anomalies in the upper mantle beneath Asia from inversion of worldwide travel time data. *Journal of Geophysical Research*, *116*, B04301. https://doi.org/10.1029/2010jb007938

Kumar, P., Yuan, X., Kind, R., & Kosarev, G. (2005). The lithosphere-asthenosphere boundary in the Tien Shan-Karakoram region from S receiver functions: Evidence for continental subduction. *Geophysical Research Letters*, *32*, L07305. https://doi.org/10.1029/2004gl022291

Laske, G., Masters, G., Ma, Z., & Pasyanos, M. (2013). *Update on CRUST1.0-A 1-degree global model of Earth's crust*. Paper presented at the European Geosciences Union General Assembly 2013, Vienna, Austria.

Lei, J. (2011). Seismic tomographic imaging of the crust and upper mantle under the central and western Tien Shan orogenic belt. *Journal of Geophysical Research*, *116*, B09305. https://doi.org/10.1029/2010jb008000

Lei, J., & Zhao, D. (2007). Teleseismic P-wave tomography and the upper mantle structure of the Central Tien Shan orogenic belt. *Physics of the Earth and Planetary Interiors*, *162*(3–4), 165–185. https://doi.org/10.1016/j.pepi.2007.04.010

Li, J., Song, X., Wang, P., & Zhu, L. (2019). A generalized H-κ method with harmonic corrections on Ps and its crustal multiples in receiver functions. *Journal of Geophysical Research: Solid Earth*, *124*, 3782–3801. https://doi.org/10.1029/2018jb016356

Li, J., Zhang, J., Zhao, X., Jiang, M., Li, Y., Zhu, Z., et al. (2016). Mantle subduction and uplift of intracontinental mountains: A case study from the Chinese Tianshan Mountains within Eurasia. *Scientific Reports*, *6*(1), 1–8. https://doi.org/10.1038/srep28831

Li, Y., Shi, L., & Gao, J. (2016). Lithospheric structure across the central Tien Shan constrained by gravity anomalies and joint inversions of receiver function and Rayleigh wave dispersion. *Journal of Asian Earth Sciences*, *124*, 191–203. https://doi.org/10.1016/j.jseaes.2016.05.003

Ligorría, J. P., & Ammon, C. J. (1999). Iterative deconvolution and receiver-function estimation. *Bulletin of the Seismological Society of America*, *89*(5), 1395–1400.

Makarov, V. I. (1995). Neotectonics and geodynamics of mountain systems of Central Asia. *Quaternary International*, *25*, 19–23. https://doi.org/10.1016/1040-6182(94)00031-y

Makarov, V. I., Alekseev, D. V., Batalev, V. Y., Bataleva, E. A., Belyaev, I. V., Bragin, V. D., et al. (2010). Underthrusting of Tarim beneath the Tien Shan and deep structure of their junction zone: Main results of seismic experiment along MANAS profile Kashgar-Song-Köl. *Geotectonics*, *44*(2), 102–126. https://doi.org/10.1134/s0016852110020020

Molnar, P., & Tapponnier, P. (1975). Cenozoic tectonics of Asia: Effects of a continental collision: Features of recent continental tectonics in Asia can be interpreted as results of the India-Eurasia collision. *Science*, *189*(4201), 419–426. https://doi.org/10.1126/science.189.4201.419

Oreshin, S., Vinnik, L., Peregoudov, D., & Roecker, S. (2002). Lithosphere and asthenosphere of the Tien Shan imaged by S receiver functions. *Geophysical Research Letters*, *29*(8), 1191. https://doi.org/10.1029/2001gl014441

Porritt, R. W., & Miller, M. S. (2018). Updates to FuncLab, a Matlab based GUI for handling receiver functions. *Computers and Geosciences*, *111*, 260–271. https://doi.org/10.1016/j.cageo.2017.11.022

Reading, A., Kennett, B., & Sambridge, M. (2003). Improved inversion for seismic structure using transformed, S-wave vector receiver functions: Removing the effect of the free surface. *Geophysical Research Letters*, *30*(19), 1981. https://doi.org/10.1029/2003gl018090

Scharer, K. M., Burbank, D. W., Chen, J., Weldon, R. J., Rubin, C., Zhao, R., & Shen, J. (2004). Detachment folding in the Southwestern Tian Shan–Tarim foreland, China: Shortening estimates and rates. *Journal of Structural Geology*, *26*(11), 2119–2137. https://doi.org/10.1016/j.jsg.2004.02.016

Simonov, V. A., Sakiev, K. S., Volkova, N. I., Stupakov, S. I., & Travin, A. V. (2008). Conditions of formation of the Atbashi Ridge eclogites (South Tien Shan). *Russian Geology and Geophysics*, *49*(11), 803–815. https://doi.org/10.1016/j.rgg.2008.04.001

Sobel, E. R., & Dumitru, T. A. (1997). Thrusting and exhumation around the margins of the western Tarim basin during the India-Asia collision. *Journal of Geophysical Research*, *102*(B3), 5043–5063. https://doi.org/10.1029/96jb03267

Steffen, R., Steffen, H., & Jentzsch, G. (2011). A three-dimensional Moho depth model for the Tien Shan from EGM2008 gravity data. *Tectonics*, *30*, TC5019. https://doi.org/10.1029/2011tc002886

Svenningsen, L., & Jacobsen, B. H. (2004). Comment on "Improved inversion for seismic structure using transformed, S-wave vector receiver functions: Removing the effect of the free surface" by Anya Reading, Brian Kennett, and Malcolm Sambridge. *Geophysical Research Letters*, *31*, L24609. https://doi.org/10.1029/2004gl021413

Sychev, I. V., Koulakov, I., Sycheva, N. A., Koptev, A., Medved, I., El Khrepy, S., & Al-Arifi, N. (2018). Collisional processes in the crust of the Northern Tien Shan inferred from velocity and attenuation tomography studies. *Journal of Geophysical Research: Solid Earth*, *123*, 1752–1769. https://doi.org/10.1002/2017jb014826

Thompson, S. C., Weldon, R. J., Rubin, C. M., Abdrakhmatov, K., Molnar, P., & Berger, G. W. (2002). Late Quaternary slip rates across the central Tien Shan, Kyrgyzstan, Central Asia. *Journal of Geophysical Research*, *107*(B9), 2203. https://doi.org/10.1029/2001jb000596

Tian, X., Zhao, D., Zhang, H., Tian, Y., & Zhang, Z. (2010). Mantle transition zone topography and structure beneath the central Tien Shan orogenic belt. *Journal of Geophysical Research*, *115*, B10308. https://doi.org/10.1029/2008jb006229

Vinnik, L. P., Aleshin, I. M., Kaban, M. K., Kiselev, S. G., Kosarev, G. L., Oreshin, S. I., & Reigber, C. (2006). Crust and mantle of the Tien Shan from data of the receiver function tomography. *Izvestiya, Physics of the Solid Earth*, *42*(8), 639–651. https://doi.org/10.1134/s1069351306080027

Vinnik, L. P., Reigber, C., Aleshin, I. M., Kosarev, G. L., Kaban, M. K., Oreshin, S. I., & Roecker, S. W. (2004). Receiver function tomography of the Central Tien Shan. *Earth and Planetary Science Letters*, *225*(1–2), 131–146. https://doi.org/10.1016/j.epsl.2004.05.039

Wessel, P., Smith, W. H. F., Scharroo, R., Luis, J., & Wobbe, F. (2013). Generic mapping tools: Improved version released. *Eos, Transactions American Geophysical Union*, *94*(45), 409–410. https://doi.org/10.1002/2013eo450001

Yang, Y., & Liu, M. (2002). Cenozoic deformation of the Tarim plate and the implications for mountain building in the Tibetan Plateau and the Tian Shan. *Tectonics*, *21*(6), 1059. https://doi.org/10.1029/2001tc001300

Yin, A., Nie, S., Craig, P., Harrison, T. M., Ryerson, F. J., Qian, X., & Yang, G. (1998). Late Cenozoic tectonic evolution of the southern Chinese Tian Shan. *Tectonics*, *17*(1), 1–27. https://doi.org/10.1029/97tc03140

Yu, Y., Zhao, D., & Lei, J. (2017). Mantle transition zone discontinuities beneath the Tien Shan. *Geophysical Journal International*, *211*(1), 80–92. https://doi.org/10.1093/gji/ggx287

Zhu, L., & Kanamori, H. (2000). Moho depth variation in southern California from teleseismic receiver functions. *Journal of Geophysical Research*, *105*(B2), 2969–2980. https://doi.org/10.1029/1999jb900322

Zhu, L., Mitchell, B. J., Akyol, N., Cemen, I., & Kekovali, K. (2006). Crustal thickness variations in the Aegean region and implications for the extension of continental crust. *Journal of Geophysical Research*, *111*, B01301. https://doi.org/10.1029/2005jb003770

Zubovich, A. V., Wang, X., Scherba, Y. G., Schelochkov, G. G., Reilinger, R., Reigber, C., et al. (2010). GPS velocity field for the Tien Shan and surrounding regions. *Tectonics*, *29*, TC6014. https://doi.org/10.1029/2010tc002772